The Unusual Redox Behaviour of Ceria and its Interaction with Hydrogen

Adam H. Clark[1*#], Kevin A. Beyer[2], Shusaku Hayama[3], Timothy I. Hyde[4], Gopinathan Sankar[1*]

1. Department of Chemistry, University College London, 20 Gordon Street, London WC1H 0AJ, United Kingdom

2. X-ray Science Division, Advanced Photon Source, Argonne National Laboratory, Lemont, Illinois 60439, United States

3. Diamond Light Source, Harwell Science & Innovation Campus, Didcot, Oxfordshire OX11 0DE, United Kingdom

4. Johnson Matthey Technology Centre, Blount's Court, Sonning Common, Reading RG4 9NH, United Kingdom

#. Current address: Paul Scherrer Institut, Villigen, CH-5232 Switzerland

ABSTRACT: The reaction between ceria and hydrogen has been subject to numerous theoretical and experimental studies due to its importance as a catalytic material. Here we present dynamic and reversible evolution of the cerium oxidation states observed through X-ray Absorption Spectroscopy experiments in addition to the investigation of associated lattice expansion and contraction through X-ray diffraction and PDF methods. Employing a novel calculation of the temperature dependence of the Gibbs free energy through consideration of the relationship between the instantaneous thermal lattice expansion and the rate of change of the cerium oxidation state, the unusual redox chemistry is reported here. This unusual behaviour is interpreted as due to the formation of a metastable cerium oxyhydride as suggested.

I. INTRODUCTION

Ceria has found numerous applications in modern catalytic processes[1–6] chief of which is as a critical component in three-way catalysts for auto-exhaust emission after-treatment due to its performance as an oxygen storage/regulator material[7,8] and as support enhancing the lifetime of catalytically active noble metal nanoparticles[6,8–14]. The catalytic properties of ceria-based materials has long been established to arise from the nature of cerium to be stable within both the Ce(III) and Ce(IV) oxidation states[5]. Whilst in the presence of noble metal nanoparticles the redox chemistry of ceria within a hydrogen atmosphere has been demonstrated to result in the removal of oxygen and formation of vacancies causing the reduction of Ce(IV) ions present in the fluorite lattice[9,15].

However in the absence of noble metal catalysts several studies have identified that the reaction of hydrogen with ceria leads to the inclusion of hydrogen into the fluorite lattice[16–23]. Fierro et al[21] established through NMR, ESR and XRD studies, identified that hydrogen is incorporated within the ceria lattice through bonding to lattice site oxygen forming a hydroxyl within the central cavity of the fluorite lattice. Recently Wu et al[23], using inelastic neutron spectroscopy, demonstrated that H_2 is activated on ceria through heterolytic dissociation forming intermediate cerium hydride and surface hydroxyl species with subsequent migration into the bulk. The presence of cerium oxyhydride species have been investigated in both experimental and first principles theoretical methods. Sohlberg et al[22] identified that below 665 K the uptake of hydrogen is a spontaneous reaction resulting in the formation of cerium oxyhydride. Meanwhile several studies exploring oxidative steam reforming of ethanol on nickel supported ceria catalysts[16,17,19,20] have found that ceria based nano-oxyhydrides to be active towards the production of H_2 at temperatures in excess of 523 K through heterolytic dissociation of ethanol. More recently ceria has been studied for its exceptional activity and selectivity towards hydrogenation reactions[24–30]. Therefore studying the interactions of hydrogen with ceria is of paramount importance in understanding the catalytic activity of Ceria in a wide array of functionality.

To probe the reaction of hydrogen with Ceria, we employed X-ray Absorption Near Edge Structure (XANES) at the Ce L3 edge using High Energy Resolution Fluorescence Detected method (HERFD). Ce L3 edge XAS is sensitive to changes in the oxidation state and electronic structure of the absorbing Ce ion. This *in situ* study allowed us to elucidate the direct observation of temperature dependent reversible Ce(IV)/Ce(III) formation in hydrogen atmosphere. In addition, time resolved X-ray total scattering methods (XTS) (2 s per spectrum) experiments were performed to follow the changes in the lattice parameter of ceria induced by the reaction with hydrogen during heating and cooling in a hydrogen atmosphere. Here we report the changes in

electronic and geometric state of ceria during the reaction with hydrogen. Specifically, evidence is presented for an apparent temperature reversible reduction and oxidation of Ce(IV) to Ce(III) and back to Ce(IV) observed by Ce L3-edge XANES and the associated dynamic lattice restructuring determined from XTS studies. This observation could be related to the formation of a meta-stable cerium oxyhydride phase[18,23,31–33].

II. RESULTS AND DISCUSSION

The complex redox chemistry of ceria was investigated using a high surface area ceria sample (136m²/g). The high surface area nature is beneficial due to the ratio of exposed surface to bulk allowing for enhanced interaction with hydrogen in the gas phase. The purity of the sample was investigated using ICP with no significant impurities detected and the results are summarized in supplementary information **Table T1.** A temperature programmed reduction (TPR) experiment was performed to monitor the consumption of hydrogen on the same sample investigated in the synchrotron based studies and it is shown in **Figure 1**.

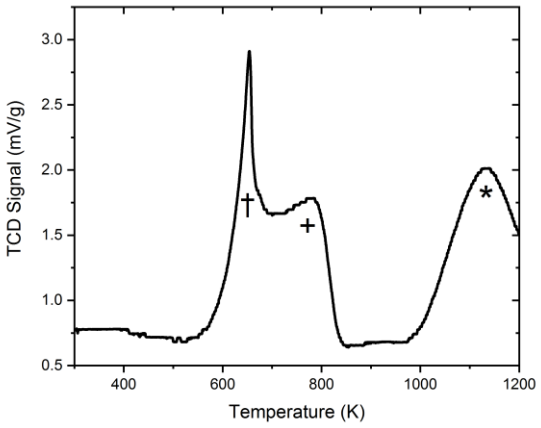

Figure 1. H_2 temperature programmed reduction demonstrating the uptake of hydrogen by the high surface area ceria sample. The peak between 600 K (†) and 800 K (+) has in this work be associated to surface changes and to the formation of a meta-stable Ce(III) species which occurs at these temperatures. Whilst the higher temperature peak (*) have been associated to the irreversible reduction of CeO_2 to Ce_2O_3.

TPR shows hydrogen consumption is observed around 600 K followed by a second peak below 800K. The consumption of hydrogen at around 600 K (†) to 800 K (+) is believed to be associated to changes at the surface of ceria and may also correspond to the formation of a meta-stable Ce(III) species which occurs at these temperatures. At temperatures above 1000 K a further hydrogen consumption is seen associated to be bulk reduction of CeO_2 to Ce_2O_3.

To follow the change in Cerium oxidation state due to the reaction of hydrogen with CeO_2, Ce L_3 edge XAS was performed. XAS methods can readily be used to probe the *in situ* redox properties of ceria and to determine the oxidation state of cerium with a high degree of certainty using HERFD-XANES. Here we undertook quantitative assessment of the proportion of Ce(IV) and Ce(III) using Ce L3-edge XANES through a peak fitting methodology[34–36], possible due to the high energy resolution achievable using HERFD-XANES techniques[34,37,38].

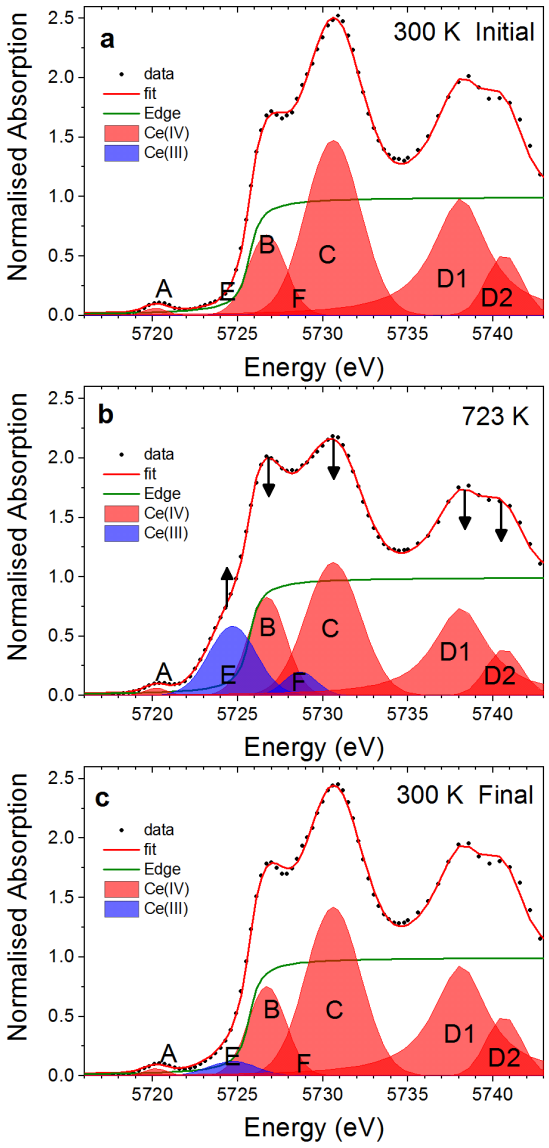

Figure 2. HERFD-XANES obtained on the high surface area ceria sample illustrating the fitted peak components **a)** 300 K prior to exposure to H_2, **b)** during exposure to H_2 at 723 K and **c)** after cooling the sample in H_2 and recorded at 300 K. Red shaded peaks represent Ce(IV) with Ce(III) indicated by blue shaded peaks.

Here feature **A** is a pre-edge feature associated to the transition from 2p core-level to the partially occupied 4f electron state within the Ce ions while **B** and **C** are associated with the $2p \rightarrow 4f^0,5d$ transition, resulting from the crystal-field splitting within cubic fluorite structure. **D1** and **D2** relate to the unscreened excited states exhibiting crystal field splitting, and **E** and F relate to Ce(III) state XANES features[39,40]. The ratio of peak areas gives the proportion of cerium oxidation states present in the system. The initial starting material can evidently be seen to contain solely Ce(IV) (red peaks) and therefore its contribution to the Ce

L3 XANES spectra (see **Figure 2a).** However upon heating to 723 K, within a 3.5%H_2/N_2 atmosphere, the presence of Ce(III) is noted (blue peaks), **Figure 2b.**Taking the peak area ratio between Ce(III) and Ce(IV) contributions, the proportion of Ce(III) at 723 K is estimated to be 15±2 %. Upon cooling to 300 K (see **Figure 2c),** whilst maintaining the 3.5%H2/N2 atmosphere, a remarkable change is seen in the XANES spectra, resembling the starting material, suggesting that the re-oxidation of Ce(III) to Ce(IV) ions takes place. Previous reports have identified that reaction with hydrogen at temperatures above *ca* 423K induces a partial reduction of Ce(IV) to Ce(III)[41–44], often interpreted as a formation of oxygen vacancies within the ceria induced by the temperature assisted, irreversible extraction of oxygen from the ceria lattice, possibly as water molecules. However, the formation of oxygen vacancies, and associated oxygen extraction from the ceria lattice, would result in a irreversible change in the **cerium** oxidation state from Ce(IV) to Ce(III).

$$CeO_2 + xH_2 \rightarrow CeO_{2-x} + xH_2O$$

Therefore the oxidation of Ce(III) to Ce(IV) during cooling in hydrogen evidences that the majority of the Ce(IV) reduction occurring through an alternative process other than the removal of oxygen from the ceria lattice. Mamotov et al[45] reported that Oxygen ions can migrate to interstitial positions leaving vacancies near the cerium ions and some evidence is also given for localisation of electrons forming a Ce(III)-vacancy complex[46].

To provide further insight into the unusual redox chemistry of the high surface area ceria sample, time resolved XAS was performed in transmission geometry (although lower resolution in energy, this study provides good time/temperature resolution as opposed to static measurements conducted at different temperatures using high-resolution HERFD technique. Example data quality is shown in **Figure S1**). To access the change in oxidation state information, a linear combination fitting analysis was performed using the starting ceria sample as the Ce(IV) reference and cerium nitrate hexahydrate (shown in Figure **S2**) for the Ce(III) reference. The use of the starting material for the Ce(IV) reference follows from the HERFD-XANES observation.

The results of the linear combination fitting, shown in **Figure 3a** demonstrate a clear hysteresis in regards to the formation of Ce(III) during reaction with hydrogen at elevated temperature and the subsequent reformation of Ce(IV) during the cooling phase of the experiment. The formation of Ce(III) within the ceria lattice can be seen to occur at temperatures above 600 K through consideration of the inflection in the derivative of the Ce(III) concentration fraction during heating, Figure **3b**. During cooling the reformation of Ce(IV) displays a minimum in the derivative of Ce(III) concentration fraction at approximately 480 K suggesting significant undercooling is required. The XAS results suggest the localisation of an electron on the Ce(IV) ion occurs during heating in hydrogen to form Ce(III) in line with the proposed model[46]Significantly here the results of the LCF analysis of standard transmission geometry XAS experiments yields an identical ~15% Ce(III) formation as observed from peak area ratio analysis of the HERFD-XANES. This suggests that both applied methods (static and dynamic change in temperature) can accurately quantify the Ce(III) formation resulting from the interaction of ceria with hydrogen at elevated temperatures and reversible formation of Ce(IV) upon cooling in hydrogen.

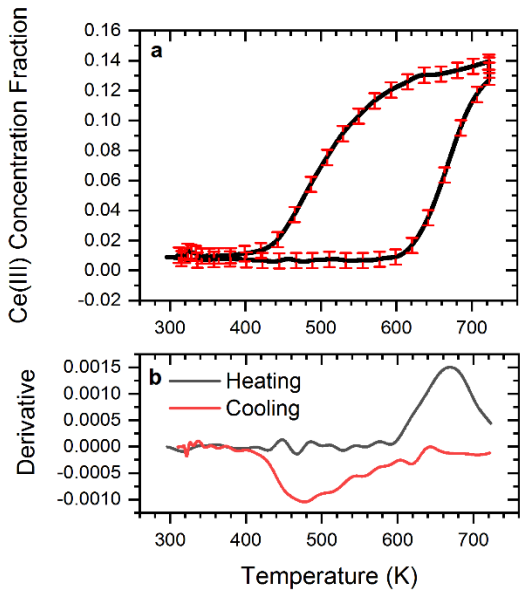

Figure 3. Results obtained from linear combination fitting performed on the time-resolved XAS measurements. **a)** Evolution with temperature of the concentration fraction of Ce(III) present within the sample during exposure to hydrogen **b)** First derivative of the plot in **a)** is given here. Ce(III) concentration fraction during the heating and cooling phases plotted in black and red respectively. A surface map of the XANES region is given in **Figure S1.**

From these observations we propose that oxygen is not removed from the ceria lattice by reaction with hydrogen at temperatures at least below 723K due to the temperature reversible nature of the Ce(IV) → Ce(III) → Ce(IV) formation. Whilst XAS provides direct access to the oxidation state of cerium within ceria and can demonstrate conclusively that the formation of Ce(III) by mild reductive processes and infers that oxygen is not removed from the ceria lattice, X-ray scattering techniques can provide in-depth information on the lattice structure. Here we have employed XTS techniques to provide insight into the lattice structure changes due to mild reduction by hydrogen. Using XTS the expansion or contraction of the ceria lattice can be used to correlate with the formation of Ce(III) observed by Ce L_3 edge XAS.. Previous studies have identified that the lattice expansion of ceria is linearly proportional to Ce(III) content within oxygen deficient ceria[47–49]. The ionic radius of Ce(III) is larger than that of Ce(IV)[50]. Therefore X-ray diffraction (XRD) analysis refining the lattice pa-

rameter of ceria gives an indirect indication of the oxidation state of cerium. Through analysis of the instantaneous expansion coefficient the deconvolution of expansion due to the formation of Ce(III) and linear thermal expansion behaviour can be achieved;

$$\alpha(T) = \frac{1}{L}\frac{dl}{dT}$$

here α gives the linear thermal expansion coefficient, L is the room temperature lattice parameter, dl/dT gives the derivative of the change in ceria lattice parameter with temperature. Ceria has been noted to have a linear thermal expansion coefficient of approximately 10×10^{-6} K^{-1},[51–53] expansion above this can be solely attributed to the formation of Ce(III). The linear thermal expansion coefficient of the high surface area ceria sample has been determined to be 9.1×10^{-6} K^{-1} (given in **Figure S3**) by an experiment performed during heating of the ceria sample in an oxygen atmosphere. This experiment also serves to corroborate the unusual ceria redox chemistry observed by XAS experiments requires a reductive environment and cannot be observed simply by heating in non-reductive atmosphere. Therefore any temperature induced formation of interstitial oxygen atoms is also not expected to give rise to reversible Ce(III) formation. **Figure 4** overlays the Rietveld refined lattice parameter during heating with the instantaneous expansion coefficient demonstrating a noticeable inflection point at approximately 600 K in agreement with the time resolved XAS results shown in **Figure 2**.

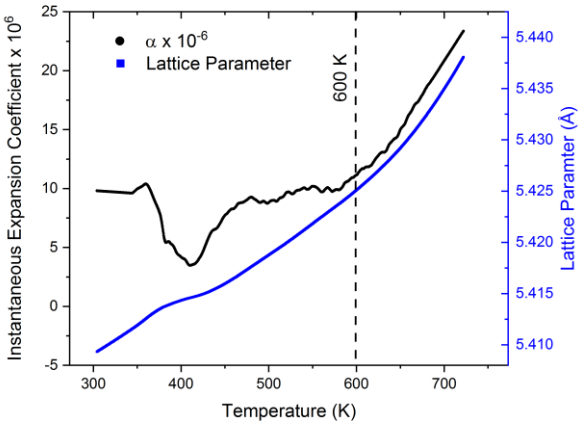

Figure 4. Expansion of the ceria lattice parameter refined using Rietveld refinement during heating (blue) with overlay displaying the calculated instantaneous expansion coefficient (black).

The contraction observed at temperatures of ca 373K, here, has been attributed to the removal of surface absorbed water and carbonaceous species observed using mass spectrometry and gravimetric analysis shown in **Figure 5**. The presence of carbonaceous species and OH has also been observed in *ex situ* infra-red data shown in **Figure S4.** Significantly no production of water is observed above 550 K. This demonstrates that the non-linear ceria lattice expansion and associated formation of Ce(III) ions above 600 K is unlikely to be due to the removal of oxygen from the lattice and formation of water by reaction of hydrogen with lattice oxygen.

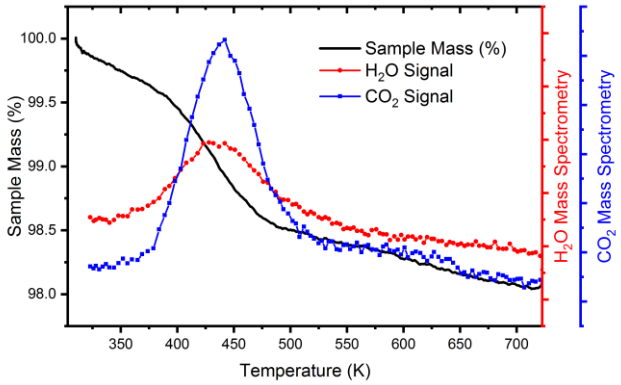

Figure 5. Gravimetric analysis showing the loss in sample mass occurring at circa 450 K (black). The blue and red traces gives the online MS signals for CO_2 and H_2O demonstrating maxima coinciding with the loss of mass from the sample at 450 K.

In addition to the extraction of lattice parameters from the XTS diffraction data, we also analysed the XTS data using pair distribution function (PDF) analysis to extract the behaviour of specific atom-pairs, Ce-O (first neighbour), Ce-Ce(Second neighbour) and Ce-Ce (higher neighbour at 6.62A). This allowed us to inherently probe the distortion of the ceria lattice during reaction with hydrogen at elevated temperatures. Modelling the individual pair correlations through employing a peak fitting procedure (shown in **Figure S5**) to the pair distribution function gives a unique insight into the local structural changes that takes place within the ceria lattice. **Figure 6** illustrates the overlay of the variation in 1st Ce-O distance at 2.34 Å, 1st Ce-Ce distance at 3.82 Å and the Ce-Ce distance at 3rd 6.62 Å, with temperature; in addition, along with these data, we also show the plot of change in lattice parameter estimated from Rietveld refinement of the diffraction data (example Rietveld refinement is shown in **Figure S6**),, in parts **a**, **b** and **c,** respectively. Here, it is evident that the overall trend in the expansion of the atom-pair correlations during heating mimics the lattice parameter changes observed by X-ray diffraction data. Whilst the lattice parameter changes shows the overall long range structural order of the fluorite lattice, PDF methods represents the local distortions present due to the reaction with hydrogen.

Considering the cooling cycle of the experiment, a local structural distortion is seen above the long-range lattice expansion, observed from XRD due to the reduction of the cerium ions. The 1st Ce-O pair correlation at approximately 2.34 Å exhibits a significant difference compared to the observed lattice parameter changes, suggesting a lengthening of the Ce-O bond; whilst the scatter of the Ce-O distance estimation is much larger than the other Ce-Ce distances, they are found to be well above the lattice parameter changes. The scattering factor of O is much weaker than that of Ce resulting in increased uncertainty in the refinement of the Ce-O pair correlation. This local distortion can

be seen to have a minor effect on the neighbouring cerium atom, as seen from the 1st Ce-Ce pair correlation. Long range order effect can be seen to be recovered at these distances of 6.62 Å with the 3rd Ce-Ce pair correlation overlaying without deviation from the XRD refined lattice parameter.

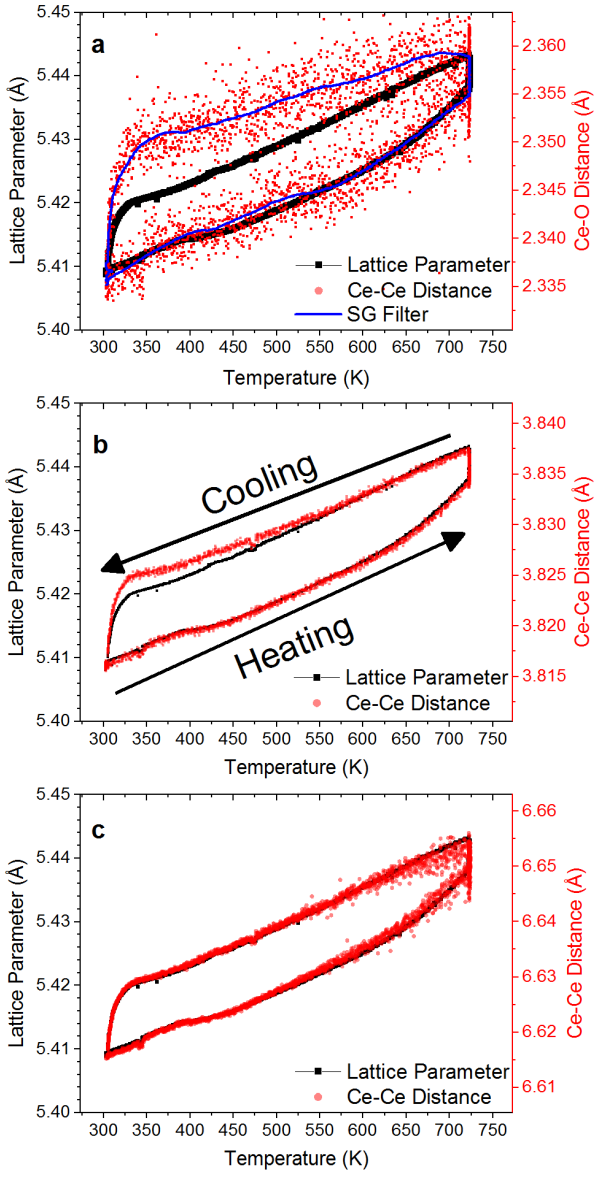

Figure 6. Overlay of PDF peak fitting (red) to XRD refined lattice parameter (black) during exposure to H_2 **a)** Ce-O pair correlation at ~2.34 Å, the blue line depicts an applied Savitzky-Golay filter to the peak fitting results for purposes of clarity, **b)** 1st Ce-Ce pair correlation at ~3.82 Å **c)** 3rd Ce-Ce pair correlation at ~6.62 Å

In ceria, oxygen has been noted to be highly mobile and has been previously suggested to readily form defect structures whereby oxygen can migrate to interstitial octahedral sites and result in the formation of Ce(III) ions[21]. Our results from the XAS experiments demonstrate that Ce(III) are formed at elevated temperatures and converted back to Ce(IV), upon cooling below ca 373K, even in an reducing atmosphere, suggesting oxygen is not removed from the ceria lattice.

This supports the possible migration of oxygen ions to an interstitial position leaving its conventional coordination environment with Ce ions. XTS results indeed support the XAS observation that changes in local structure and observed lattice parameter change indicate the reversible redox reaction of Ce(IV) to Ce(III) and back to Ce(IV) upon cooling. XTS experiments have also demonstrated that the expansion of ceria is linear with heating in the absence of a reductive atmosphere (**Figure S3**) and thus the linear thermal expansion is not as a result of oxygen migration into interstitial octahedral sites. In the presence of hydrogen a non-linear expansion above 600 K of the ceria lattice has been observed and is shown to result in a local distortion. Based on these observation we propose that reaction of hydrogen with ceria results in the reversible reduction of Ce(IV) to Ce(III) and a distortion in the local structure due to the inclusion of hydrogen into the ceria lattice in a method similar to that proposed by Fierro *et al*[21]. Elsewhere, it has also been reported that under mild reduction with hydrogen a cerium oxyhydride or cerium hydride phase can be formed[16,21–23].

With the observed local structural changes, partial changes in the oxidation state of Ce(IV) to Ce(III) and the ceria lattice relaxing upon cooling we propose that hydrogen inclusion into the ceria lattice occurs at elevated temperatures forming a metastable structure. Such behaviour has not been observed when heating in an oxygen atmosphere (**Figure S3**). We propose that the suggested complex Ce(III)-Oxygen vacancy[46] coupled with an inclusion of hydrogen into the ceria lattice forming internal OH structures resulting in a cerium oxyhydride phase, H_xCeO_2 in the surface and subsurface layers of the Ceria leading to this unusual redox observations seen XAS and XTS measurements at elevated temperature.

III. MODELLING OF LATTICE EXPANSION

When considering the interactions with hydrogen the formation hydroxyl groups within the ceria lattice or on surface layers provide a possible mechanism for the Ce(III) formation. The formation of a bulk cerium oxyhydride has previously been proposed in a first principles theoretical study by Sohlberg *et al*[22] demonstrating that the uptake of hydrogen into the ceria through the formation of hydroxyl groups:

$$\boldsymbol{Ce_4O_8 + \frac{x}{2}H_2 \rightarrow H_xCe_4O_8}$$

Such that one can establish the temperature dependence on the change in Gibbs free energy by approximating that the inclusion of hydrogen into the ceria lattice only results in a minor perturbation of the enthalpy of the fluorite lattice and that H_2 only appreciably contributes to the change in entropy from computation methods.

$$\boldsymbol{\Delta G(T) = \Delta H - T\Delta S}$$

whereby a negative value for the change in Gibbs free energy favours the spontaneous formation of cerium oxyhydride. Furthermore the probability of a ceria unit cell containing a hydrogen atom to form a cerium oxyhydride phase can be established as a function of the temperature dependent change in Gibbs free energy[22,54] such that;

$$\boldsymbol{\rho(T)} = \frac{e^{\frac{-\Delta G(T)}{kT}}}{1 + e^{\frac{-\Delta G(T)}{kT}}}$$

where k is given as the Boltzmann constant. Here we propose that the derivative of the probability for hydrogen inclusion into the ceria lattice is directly proportional to the instantaneous expansion coefficient of the ceria lattice. This can be rationalised by considering the probability for the formation of cerium oxyhydride directly yielding the proportion of cerium present in the Ce(III) oxidation state and as such can be used to model the degree of lattice expansion due to the presence of hydrogen within the ceria lattice. Through this method one can consider that the rate expansion of the ceria lattice above that of thermal expansion to be proportional to the derivative of the probability for the formation of cerium oxyhydride such that;

$$\boldsymbol{\alpha(T)} = \boldsymbol{\alpha_{T_0}(T)} + \boldsymbol{C}\frac{\boldsymbol{d\rho(T)}}{\boldsymbol{dT}}$$

where C gives the maximal expansion due to the formation of Ce(III) and $\boldsymbol{\alpha_{T_0}(T)}$ gives the linear thermal expansion coefficient of ceria; demonstration of the thermal dependence on the linear thermal expansion coefficient of ceria under an oxygen atmosphere is presented in the supplementary information and has been observed previously elsewhere[51–53]. Therefore through a least squares minimisation strategy, result shown in **Figure 7**, it is thus possible to establish the temperature dependence of the change in Gibbs free energy and establish ΔH and ΔS for the formation of cerium oxyhydride directly from the dynamic expansion of the ceria lattice and as such note that the formation of cerium oxyhydride is spontaneous in temperatures above 815 K.

$$\boldsymbol{\Delta G(T) = 0.76(3) - 9.35(5)x10^{-4}T}$$

From determination of the probability for the formation of cerium oxyhydride formation at 723 K, ρ(723 K) = 0.19, it is possible to determine the number of hydrogen atoms that each $\boldsymbol{Ce_4O_8}$ can stabilise the storage of 1 hydrogen atoms by correlation with the maximum Ce(III) content observed from HERFD-XANES. The maximum Ce(III) content formed at 723 K is 15±2% and corresponds to the formation of cerium oxyhydride in the form $\boldsymbol{H_{0.6}Ce_4O_8}$. The fraction of Ce(III) formation obtained by modelling of the expansion of the ceria lattice yields a remarkable agreement with the results obtained from analysis of the XAS experiments. This behaviour would appear to be symptomatic of homolytic dissociation of H_2 producing two hydroxyl species being favourable however intermediately heterolytic dissociation may also be possible[23,31].

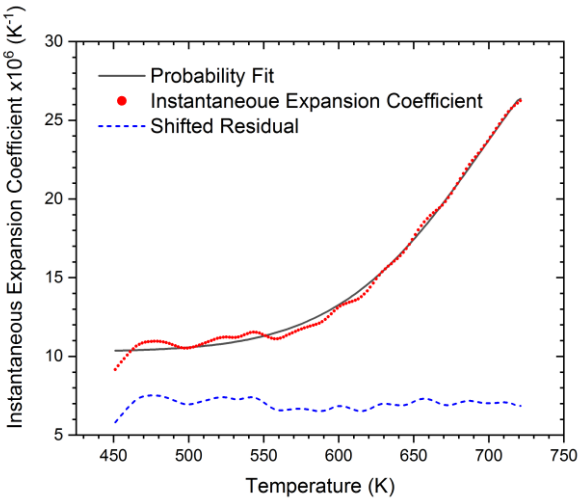

Figure 7. Probability model (red) for the instantaneous thermal expansion coefficient (black) as a function of temperature demonstrating strong agreement between expansion of the ceria lattice and uptake of hydrogen. The residual is shown below (blue) and is shifted by 7x10^6 for the purpose of figure clarity.

IV. CONCLUSIONS

Through an *in situ* XAS and time resolved XTS experimentation, we have been able to show that *ca* 15% of Ce(IV) ions are reduced to Ce(III) in the ceria lattice at elevated temperatures, in reducing atmosphere. These reduced Ce(III) ions are found to be stable only at elevated temperatures and is reoxidised upon cooling below 400 K in reducing atmosphere. This reoxidation of Ce(III) ions in reducing atmosphere clearly suggests that the oxygen atoms within the ceria lattice are not removed during the reduction in a hydrogen atmosphere at elevated temperatures.

The formation of Ce(III), observed by XANES, can be stabilised via the localisation of an electron to the cerium ion as indicated by theoretical studies[46]. When within a hydrogen atmosphere the reduction of Ce(IV) to Ce(III) is proposed to be through the formation of a cerium oxyhydride at elevated temperatures. This may arise from the formation of a hydroxyl structures in the surface and subsurface layers resulting in the lengthening of the Ce-O bond and in the localization of an electron onto the cerium ion[46].

Upon cooling to 300 K the almost total reoxidation of Ce(III) to Ce(IV) clearly demonstrates that this complex containing cerium oxyhydride is meta stable. Using XTS we have demonstrated that above 600 K an expansion of the ceria lattice is a signature of Ce(III) formation and that a local distortion occurs. Through these observations and modelling of the changes in lattice parameters and distortions seen in the local atom-pair (Ce-O in particular) correlations during the reduction and reoxidation (in hydrogen atmosphere) it is possible to propose hydrogen inclusion into the ceria lattice. In addition, through employment of a probability model governed by the temperature dependence on the Gibbs free energy for the formation of cerium oxyhydride, significant insight is achieved yielding

the result cerium oxyhydride is stable only at temperatures in excess of 600 K. Cerium oxyhydride species have been proposed to be active towards hydrogenation catalysis and in the production of hydrogen from ethanol steam reforming[19,23,24,28]. Thus one can propose that the operating temperature window for hydrogenation catalysis is at temperatures between 600 K and approximately 850 K. Above 850 K ceria is known to readily reduce in a hydrogen atmosphere to Ce_2O_3, for ceria based catalyst[55].

V. EXPERIMENTAL METHODS

The high-surface area ceria support was obtained from Rhodia-Solvay. X-ray total scattering patterns were obtained from 11IDB beamline at the APS, using a 2D detector. The wavelength was λ=0.1430 Å and with a Q range for Fourier transform to real space being between 0.55 and 27.93 $Å^{-1}$ using the xPDFsuite software[56]. The sample was prepared to produce monodisperse grain sizes to aid in gas flow over the sample. The sample was loaded into a 0.9 mm internal diameter fused silica capillary with metal furnace elements used to control the temperature mounted above and below the sample capillary. A flow rate of 3.5%H2/N2 of 30ml/min through the capillary was utilized throughout a continual ramped heating and cooling of 10 K min^{-1} between 300 K and 723 K. The samples were also held at 723 K for 10 minutes prior to cooling.

Rietveld analysis of all samples has been performed using GSAS[57] to extract the lattice parameter of the crystalline ceria phase present in the sample, an example Rietveld refinement fit is shown in **Figure S6**. GSAS was operated in batch refinement mode using a model refinement relating to the high surface area ceria support at room temperature as the starting point for all samples. The sequential fitting in batch operation takes the refined parameters from the previous fit as the starting point, as such it is possible to reduce the error on the refinements. During the XRD Rietveld refinements only the lattice parameter, thermal disorder parameters, scale factor and the background were refined. Oxygen occupancy was not explored due to the strong correlation with both the scale factor and the thermal disorder parameters.

Peak fitting to the PDF G(r) was performed using a generalised peak fitting program. A maximum radius of 10.7 Å for automatic peak searching was employed for the initial estimates of the peak positions. Baseline estimation and subtraction was undertaken using an asymmetric least squares approach. Gaussian profiles were fitted using scipy curvefit with error estimation from covariance matrix diagonalization.

HERFD-XANES measurements at the Ce L3 edge were conducted at I20-scanning beam-line at the Diamond Light source[58] on the ceria sample through monitoring the intensity of the Ce $L\alpha_1$ photo emission line at 4840 eV using the I20 high-resolution X-ray emission spectrometer, fitted with three Si(400) analyzers. In a typical experiment, about 12 mg of the sample was mixed with 50 mg of fumed silica and pressed into a pellet and loaded in to an *insitu* cell. The cell was purged with N_2 prior to heating to 723 K in a 3.5%H_2/He atmosphere followed by cooling to room temperature under the same atmosphere. Measurements were performed isothermally at 300 K prior to heating, 723 K and at 300 K after cooling.

Time-resolved XAS measurements at the Ce L3 edge were performed at the SuperXAS beamline of the SLS using the QEXAFS setup using a channel-cut Si(111) crystal monochromator. XAS spectra were obtained in transmission geometry using 15 cm ion chambers filled with 0.5 bar N_2 and 0.5 bar He. The data collection was performed with 1Hz repetition rate allowing for a temporal resolution of 1 s. Energy calibration was performed by consideration of the maximum derivative of a ceria standard material. The spectra were processed using in-house developed software employing butterworth filtering for high frequency noise reduction and interpolation onto a constant energy grid was performed using highly optimized localised radial basis function interpolation taking advantage of the oversampling in the QEXAFS setup. Linear combination fitting using the starting material and a cerium nitrate hexahydrate standard material was performed using the Presto-Pronto software package. The quality of the extracted Ce L_3 data is shown in the **Figure S1.**

Surface area measurements were performed using N_2 BET analysis using the Quantachrome Autosorb-IQ E instrument. Sample mass of approximately 500mg of the High Surface Area ceria sample was used while heating at 10 K min^{-1} up to a maximum temperature of 623 K.

Temperature Programmed Reduction (TPR) experiments were performed using an in-house built TPR/TPO rig. Approximately 200 mg of the pelletized CeO_2 sample was used. The sample was first flushed in N_2 prior to heating at 10 K min^{-1} in a 10%H_2/N_2 atmosphere to 1200 K. All gases used were flowing at 30 ml min^{-1}.

Gravimetric analysis was performed using a Hidden Gravimetric Gas Sorption Analyzer instrument. Sample mass was 102 mg of the High Surface Area ceria sample was used. The samples were, under 5% H_2/N_2 flowing at 30 ml min^{-1}, heated from 298 K to 723 K at 10 K min^{-1}.

ASSOCIATED CONTENT

Supporting Information is given showing: Example QEXAFS data and linear combination fitting. XTS analysis to determine the expansion coefficient of ceria, IR and impurity analysis of the sample. This material is available free of charge via the Internet at http://pubs.acs.org.

ACKNOWLEDGMENT

We thank EPSRC and Johnson Matthey Plc for financial support of a Case Award (AHC, EPSRC: 1635837) and Iain Hitchcock, Matthew Rose, Amy Kolpin and Hanita Gill for IGA, ICP, TPR and BET measurements respectfully. The authors would also like to thank staff from Diamond Light Source, UK (I20-Scanning) for access to beamtime under

proposal number SP16508. This research used resources of the Advanced Photon Source, a U.S. Department of Energy (DOE) Office of Science User Facility operated for the DOE Office of Science by Argonne National Laboratory under Contract No. DE-AC02-06CH11357. We would also like to acknowledge the use of the SuperXAS beamline at the SLS and the Paul Scherrer Institute for collection of the time-resolved XAS measurements.

ABBREVIATIONS

XAS, X-ray Absorption Spectroscopy; XANES, X-ray Absorption Near Edge Structure; HERFD-XANES, High Energy Resolution Fluorescence Detected X-ray Absorption Near Edge Structure; XTS, X-ray Total Scattering; PDF, Pair Distribution Function; QEXAFS, Quick scanning Extended X-ray Absorption Fine Structure; XRD, X-ray Diffraction; TPR, temperature programmed reduction; TPO, temperature programmed oxidation

REFERENCES

(1) Craciun, R.; Shereck, B.; Gorte, R. J. Kinetic Studies of Methane Steam Reforming on Ceria-Supported Pd. *Catal. Letters* **1998**, *51* (3), 149–153.

(2) Heck, R. M.; Farrauto, R. J. Automobile Exhaust Catalysts. *Applied Catalysis A: General*. 2001, pp 443–457.

(3) Matatov-Meytal, Y. I.; Sheintuch, M. Catalytic Abatement of Water Pollutants. *Ind. Eng. Chem. Res.* **1998**, *37* (2), 309–326.

(4) Pantu, P.; Kim, K.; Gavalas, G. R. Methane Partial Oxidation on Pt/CeO2-ZrO2in the Absence of Gaseous Oxygen. *Appl. Catal. A Gen.* **2000**, *193* (1–2), 203–214.

(5) Trovarelli, A. *Catalysis by Ceria and Related Materials*; Imperial College Press: London, 2002; Vol. 2.

(6) Yeung, C. M. Y.; Tsang, S. C. Noble Metal Core-Ceria Shell Catalysts for Water-Gas Shift Reaction. *J. Phys. Chem. C* **2009**, *113* (15), 6074–6087.

(7) Scanlon, D. O.; Morgan, B. J.; Watson, G. W. The Origin of the Enhanced Oxygen Storage Capacity of Ce1-x(Pd/Pt)XO2. *Phys. Chem. Chem. Phys.* **2011**, *13* (10), 4279–4284.

(8) Vayssilov, G. N.; Lykhach, Y.; Migani, A.; Staudt, T.; Petrova, G. P.; Tsud, N.; Skála, T.; Bruix, A.; Illas, F.; Prince, K. C.; et al. Support Nanostructure Boosts Oxygen Transfer to Catalytically Active Platinum Nanoparticles. *Nat. Mater.* **2011**, *10* (4), 310–315.

(9) Acerbi, N.; Golunski, S.; Tsang, S. C.; Daly, H.; Hardacre, C.; Smith, R.; Collier, P. Promotion of Ceria Catalysts by Precious Metals: Changes in Nature of the Interaction under Reducing and Oxidizing Conditions. *J. Phys. Chem. C* **2012**, *116* (25), 13569–13583.

(10) Bernal, S.; Calvino, J. J.; Cauqui, M. A.; Gatica, J. M.; Larese, C.; Pérez Omil, J. A.; Pintado, J. M. Some Recent Results on Metal/Support Interaction Effects in NM/CeO2(NM: Noble Metal) Catalysts. *Catal. Today* **1999**, *50* (2), 175–206.

(11) Graciani, J.; Vidal, A. B.; Rodriguez, J. A.; Sanz, J. F. Unraveling the Nature of the Oxide-Metal Interaction in Ceria-Based Noble Metal Inverse Catalysts. *J. Phys. Chem. C* **2014**, *118* (46), 26931–26938.

(12) Jen, H. W.; Graham, G. W.; Chun, W.; McCabe, R. W.; Cuif, J. P.; Deutsch, S. E.; Touret, O. Characterization of Model Automotive Exhaust Catalysts: Pd on Ceria and Ceria-Zirconia Supports. *Catal. Today* **1999**, *50* (2), 309–328.

(13) Lykhach, Y.; Kozlov, S. M.; Skála, T.; Tovt, A.; Stetsovych, V.; Tsud, N.; Dvořák, F.; Johánek, V.; Neitzel, A.; Mysliveček, J.; et al. Counting Electrons on Supported Nanoparticles. *Nat. Mater.* **2016**, *15* (3), 284–288.

(14) Zhou, J.; Baddorf, A. P.; Mullins, D. R.; Overbury, S. H. Growth and Characterization of Rh and Pd Nanoparticles on Oxidized and Reduced CeOx (111) Thin Films by Scanning Tunneling Microscopy. *J. Phys. Chem. C* **2008**, *112* (25), 9336–9345.

(15) Acerbi, N.; Tsang, S. C.; Golunski, S.; Collier, P. A Practical Demonstration of Electronic Promotion in the Reduction of Ceria Coated PGM Catalysts. *Chem. Commun.* **2008**, No. 13, 1578–1580.

(16) Pirez, C.; Capron, M.; Jobic, H.; Dumeignil, F.; Jalowiecki-Duhamel, L. Highly Efficient and Stable CeNiHZOY Nano-Oxyhydride Catalyst for H2 Production from Ethanol at Room Temperature. *Angew. Chemie - Int. Ed.* **2011**, *50* (43), 10193–10197.

(17) Pirez, C.; Fang, W.; Capron, M.; Paul, S.; Jobic, H.; Dumeignil, F.; Jalowiecki-Duhamel, L. Steam Reforming, Partial Oxidation and Oxidative Steam Reforming for Hydrogen Production from Ethanol over Cerium Nickel Based Oxyhydride Catalyst. *Appl. Catal. A Gen.* **2016**, *518*, 78–86.

(18) Aubriet, F.; Gaumet, J. J.; De Jong, W. A.; Groenewold, G. S.; Gianotto, A. K.; McIlwain, M. E.; Van Stipdonk, M. J.; Leavitt, C. M. Cerium Oxyhydroxide Clusters: Formation, Structure, and Reactivity. *J. Phys. Chem. A* **2009**, *113* (22), 6239–6252.

(19) Jalowiecki-Duhamel, L.; Pirez, C.; Capron, M.; Dumeignil, F.; Payen, E. Hydrogen Production from Ethanol Steam Reforming over Cerium and Nickel Based Oxyhydrides. *Int. J. Hydrogen Energy* **2010**, *35* (23), 12741–12750.

(20) Jalowiecki-Duhamel, L.; Zarrou, H.; D'Huysser, A. Hydrogen Production at Low Temperature from Methane on Cerium and Nickel Based Mixed Oxides. *Int. J. Hydrogen Energy* **2008**, *33* (20), 5527–5534.

(21) Fierro, J. L. G.; Soria, J.; Sanz, J.; Rojo, J. M. Induced Changes in Ceria by Thermal Treatments under Vacuum or Hydrogen. *J. Solid State Chem.* **1987**, *66* (1), 154–162.

(22) Sohlberg, K.; Pantelides, S. T.; Pennycook, S. J. Interactions of Hydrogen with CeO2. *J. Am. Chem. Soc.* **2001**, *123* (27), 6609–6611.

(23) Wu, Z.; Cheng, Y.; Tao, F.; Daemen, L.; Foo, G. S.; Nguyen, L.; Zhang, X.; Beste, A.; Ramirez-Cuesta, A. J. Direct Neutron Spectroscopy Observation of Cerium Hydride Species on a Cerium Oxide Catalyst. *J. Am. Chem. Soc.* **2017**, *139* (28), 9721–9727.

(24) Carrasco, J.; Vilé, G.; Fernández-Torre, D.; Pérez, R.; Pérez-Ramírez, J.; Ganduglia-Pirovano, M. V. Molecular-Level Understanding of CeO2 as a Catalyst for Partial Alkyne Hydrogenation. *J. Phys. Chem. C* **2014**, *118* (10), 5352–5360.

(25) Wang, Y. G.; Mei, D.; Glezakou, V. A.; Li, J.; Rousseau, R. Dynamic Formation of Single-Atom Catalytic Active Sites on Ceria-Supported Gold Nanoparticles. *Nat. Commun.* **2015**, *6* (1), 6511.

(26) Gill, L.; Beste, A.; Chen, B.; Li, M.; Mann, A. K. P.; Overbury, S. H.; Hagaman, E. W. Fast MAS1H NMR Study of Water Adsorption and Dissociation on the (100) Surface of Ceria Nanocubes: A Fully Hydroxylated, Hydrophobic Ceria Surface. *J. Phys. Chem. C* **2017**, *121* (13), 7450–7465.

(27) García-Melchor, M.; López, N. Homolytic Products from Heterolytic Paths in H2 Dissociation on Metal Oxides: The Example of CeO2. *J. Phys. Chem. C* **2014**, *118* (20), 10921–10926.

(28) Riley, C.; Zhou, S.; Kunwar, D.; De La Riva, A.; Peterson, E.; Payne, R.; Gao, L.; Lin, S.; Guo, H.; Datye, A. Design of Effective Catalysts for Selective Alkyne Hydrogenation by Doping of Ceria with a Single-Atom Promotor. *J. Am. Chem. Soc.* **2018**, *140* (40), 12964–12973.

(29) Werner, K.; Weng, X.; Calaza, F.; Sterrer, M.; Kropp, T.; Paier, J.; Sauer, J.; Wilde, M.; Fukutani, K.; Shaikhutdinov, S.; et al. Toward an Understanding of Selective Alkyne Hydrogenation on Ceria: On the Impact of O Vacancies on H2Interaction with CeO2(111). *J. Am. Chem. Soc.* **2017**, *139* (48), 17608–17616.

(30) Zhang, S.; Huang, Z. Q.; Ma, Y.; Gao, W.; Li, J.; Cao, F.; Li, L.; Chang, C. R.; Qu, Y. Solid Frustrated-Lewis-Pair Catalysts Constructed by Regulations on Surface Defects of Porous

Nanorods of CeO2. *Nat. Commun.* **2017**, *8*, 15266.
(31) García-Melchor, M.; López, N. Homolytic Products from Heterolytic Paths in H2 Dissociation on Metal Oxides: The Example of CeO2. *J. Phys. Chem. C* **2014**, *118* (20), 10921–10926.
(32) Sohlberg, K.; Pantelides, S. T.; Pennycook, S. J. Interactions of Hydrogen with CeO2. *J. Am. Chem. Soc.* **2001**, *123* (27), 6609–6611.
(33) Matsukawa, T.; Hoshikawa, A.; Niwa, E.; Yashima, M.; Ishigaki, T. Crystal Structure of Blue-Colored Ceria during Redox Reactions in a Hydrogen Atmosphere. *CrystEngComm* **2018**, *20* (2), 155–158.
(34) Paun, C.; Safonova, O. V.; Szlachetko, J.; Abdala, P. M.; Nachtegaal, M.; Sa, J.; Kleymenov, E.; Cervellino, A.; Krumeich, F.; Van Bokhoven, J. A. Polyhedral CeO2nanoparticles: Size-Dependent Geometrical and Electronic Structure. *J. Phys. Chem. C* **2012**, *116* (13), 7312–7317.
(35) Soldatov, A. V.; Ivanchenko, T. S.; Della Longa, S.; Kotani, A.; Iwamoto, Y.; Bianconi, A. Crystal-Structure Effects in the Ce L3-Edge x-Ray-Absorption Spectrum of CeO2: Multiple-Scattering Resonances and Many-Body Final States. *Phys. Rev. B* **1994**, *50* (8), 5074–5080.
(36) Marchbank, H. R.; Clark, A. H.; Hyde, T. I.; Playford, H. Y.; Tucker, M. G.; Thompsett, D.; Fisher, J. M.; Chapman, K. W.; Beyer, K. A.; Monte, M.; et al. Structure of Nano-Sized CeO2Materials: Combined Scattering and Spectroscopic Investigations. *ChemPhysChem* **2016**, *17* (21), 3494–3503.
(37) Hämäläinen, K.; Siddons, D. P.; Hastings, J. B.; Berman, L. E. Elimination of the Inner-Shell Lifetime Broadening in x-Ray-Absorption Spectroscopy. *Phys. Rev. Lett.* **1991**, *67* (20), 2850–2853.
(38) Reinhardt, F.; Beckhoff, B.; Eba, H.; Kanngiesser, B.; Kolbe, M.; Mizusawa, M.; Muüller, M.; Pollakowski, B.; Sakurai, K.; Ulm, G. Evaluation of High-Resolution X-Ray Absorption and Emission Spectroscopy for the Chemical Speciation of Binary Titanium Compounds. *Anal. Chem.* **2009**, *81* (5), 1770–1776.
(39) Cafun, J. D.; Kvashnina, K. O.; Casals, E.; Puntes, V. F.; Glatzel, P. Absence of Ce3+ Sites in Chemically Active Colloidal Ceria Nanoparticles. *ACS Nano* **2013**, *7* (12), 10726–10732.
(40) Safonova, O. V; Guda, A. A.; Paun, C.; Smolentsev, N.; Abdala, P. M.; Smolentsev, G.; Nachtegaal, M.; Szlachetko, J.; Soldatov, M. A.; Soldatov, A. V; et al. Electronic and Geometric Structure of Ce3+ Forming under Reducing Conditions in Shaped Ceria Nanoparticles Promoted by Platinum. *J. Phys. Chem. C* **2014**, *118* (4), 1974–1982.
(41) Haigh, S. J.; Young, N. P.; Sawada, H.; Takayanagi, K.; Kirkland, A. I. Imaging the Active Surfaces of Cerium Dioxide Nanoparticles. *ChemPhysChem* **2011**, *12* (13), 2397–2399.
(42) Garvie, L. A. J.; Buseck, P. R. Determination of Ce4+/Ce3+ in Electron-Beam-Damaged CeO2 by Electron Energy-Loss Spectroscopy. *J. Phys. Chem. Solids* **1999**, *60* (12), 1943–1947.
(43) Gilliss, S. R.; Bentley, J.; Carter, C. B. Electron Energy-Loss Spectroscopic Study of the Surface of Ceria Abrasives. In *Applied Surface Science*; North-Holland, 2005; Vol. 241, pp 61–67.
(44) Costantini, J. M.; Miro, S.; Touati, N.; Binet, L.; Wallez, G.; Lelong, G.; Guillaumet, M.; Weber, W. J. Defects Induced in Cerium Dioxide Single Crystals by Electron Irradiation. *J. Appl. Phys.* **2018**, *123* (2), 025901.
(45) Mamontov, E.; Egami, T.; Brezny, R.; Koranne, M.; Tyagi, S. Lattice Defects and Oxygen Storage Capacity of Nanocrystalline Ceria and Ceria-Zirconia. *J. Phys. Chem. B* **2000**, *104* (47), 11110–11116.
(46) Skorodumova, N. V; Simak, S. I.; Lundqvist, B. I.; Abrikosov, I. A.; Johansson, B. Quantum Origin of the Oxygen Storage Capability of Ceria. *Phys. Rev. Lett.* **2002**, *89* (16), 166601/1-166601/4.
(47) Kim, D. -J. Lattice Parameters, Ionic Conductivities, and Solubility Limits in Fluorite-Structure MO2Oxide [M = Hf4+, Zr4+, Ce4+, Th4+, U4+] Solid Solutions. *J. Am. Ceram. Soc.* **1989**, *72* (8), 1415–1421.
(48) Campserveux, J.; Gerdanian, P. Etude Thermodynamique de l'oxyde CeO2-Xpour 1.5 < O Ce < 2. *J. Solid State Chem.* **1978**, *23* (1–2), 73–92.
(49) Panhans, M. A.; Blumenthal, R. N. A Thermodynamic and Electrical Conductivity Study of Nonstoichiometric Cerium Dioxide. *Solid State Ionics* **1993**, *60* (4), 279–298.
(50) Shannon, R. D. Revised Effective Ionic Radii and Systematic Studies of Interatomic Distances in Halides and Chalcogenides. *Acta Crystallogr. Sect. A* **1976**, *32* (5), 751–767.
(51) GUPTA, M. L.; SINGH, S. Thermal Expansion of CeO2, Ho2O3, and Lu2O3from 100° to 300°K by an X-Ray Method. *J. Am. Ceram. Soc.* **1970**, *53* (12), 663–665.
(52) Hayashi, H. Thermal Expansion of Gd-Doped Ceria and Reduced Ceria. *Solid State Ionics* **2000**, *132* (3–4), 227–233.
(53) Hayashi, H.; Saitou, T.; Maruyama, N.; Inaba, H.; Kawamura, K.; Mori, M. Thermal Expansion Coefficient of Yttria Stabilized Zirconia for Various Yttria Contents. *Solid State Ionics* **2005**, *176* (5–6), 613–619.
(54) Van De Walle, C. G.; Laks, D. B.; Neumark, G. F.; Pantelides, S. T. First-Principles Calculations of Solubilities and Doping Limits: Li, Na, and N in ZnSe. *Phys. Rev. B* **1993**, *47* (15), 9425–9434.
(55) Yao, H. C.; Yao, Y. F. Y. Ceria in Automotive Exhaust Catalysts. I. Oxygen Storage. *J. Catal.* **1984**, *86* (2), 254–265.
(56) Yang, X.; Juhas, P.; Farrow, C. L.; Billinge, S. J. L. XPDFsuite: An End-to-End Software Solution for High Throughput Pair Distribution Function Transformation, Visualization and Analysis. arXiv:1402.3163v3 [cond-mat] 2014 https://arxiv.org/abs/1402.3163 (accessed 29.08.2019)
(57) Toby, B. H. EXPGUI, a Graphical User Interface for GSAS. *J. Appl. Crystallogr.* **2001**, *34* (2), 210–213.
(58) Hayama, S.; Duller, G.; Sutter, J. P.; Amboage, M.; Boada, R.; Freeman, A.; Keenan, L.; Nutter, B.; Cahill, L.; Leicester, P.; et al. The Scanning Four-Bounce Monochromator for Beamline I20 at the Diamond Light Source. *J. Synchrotron Radiat.* **2018**, *25* (5), 1556–1564.
(59) Ravel, B.; Newville, M. ATHENA, ARTEMIS, HEPHAESTUS: Data Analysis for X-Ray Absorption Spectroscopy Using IFEFFIT. In *Journal of Synchrotron Radiation*; 2005; Vol. 12, pp 537–541.

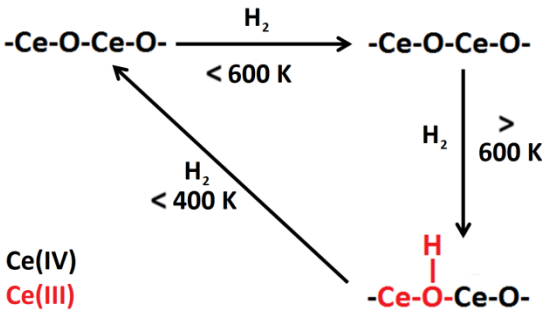
-Ce-O-Ce-O-
H2
< 600 K
-Ce-O-Ce-O-
H2
>
600 K
H2
< 400 K
H
-Ce-O-Ce-O-
Ce(IV)
Ce(III)